# Analytical Methods

Accepted Manuscript


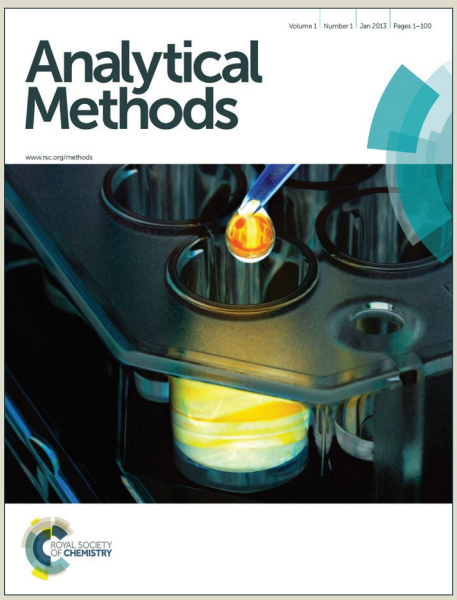


This is an *Accepted Manuscript*, which has been through the Royal Society of Chemistry peer review process and has been accepted for publication.

*Accepted Manuscripts* are published online shortly after acceptance, before technical editing, formatting and proof reading. Using this free service, authors can make their results available to the community, in citable form, before we publish the edited article. We will replace this *Accepted Manuscript* with the edited and formatted *Advance Article* as soon as it is available.

You can find more information about *Accepted Manuscripts* in the Information for Authors.




ROYAL SOCIETY OF CHEMISTRY

www.rsc.org/methods

# Designing and application of screen-printed bulk modified electrodes using anthraquinone moiety/cysteamine functionalized-gold nanoparticle for the detection of dissolved oxygen

Ida Tiwari[1], Monali Singh[1], Mandakini Gupta[1], Jonathan P. Metters[2] and Craig E. Banks[2]

[1]*Centre of Advanced Study in Chemistry, Faculty of Science, Banaras Hindu University, Varanasi (INDIA)*

[2]*Faculty of Science and Engineering, School of Science and the Environment, Division of Chemistry and Environmental Science, Manchester Metropolitan University, Chester Street, Manchester, M15GD, Lancs., UK*

**Abstract:**

The present research investigation focuses on the electroanalytical sensing of dissolved oxygen using disposable and economic nanostructure based screen-printed bulk modified electrodes. A gold nanoparticle based nanostructure of anthraquinone derivative and cysteamine was prepared. The prepared nanostructred material was morphologically characterized using transmission electron microscopy while the other physical characterization was done by energy dispersive X-ray spectroscopy. The prepared material was further employed in graphite ink for development of next generation sensors that can be mass produced at an economical rate so as to develop technology from the laboratory into the field. The electroanalytical determination of dissolved oxygen is found to be possible over the concentration range of 0.2 mg/L to 6.1 mg/L with a detection limit of 0.131 mg/L (based on 3-sigma). We demonstrate proof-of-concept that this approach provides a rapid and inexpensive sensing strategy for determining dissolved oxygen in contaminated water samples.

**Key words:** screen-printed electrodes, dissolved oxygen, gold nanoparticles, anthraquinone

**Introduction:**

Concern over environmental pollution and health issues have motivated scientist for significant research, and efforts are on for the development of technology to address these issues. Worldwide research is going on by the desire to not only measure the dissolved oxygen for the medical applications such as the oxygen content in blood and tissues but also to monitor the impact of effluents coming from various industries by measuring the amount of dissolved oxygen in natural and industrial waters. Dissolved oxygen is an important water quality parameter as it is necessary for good water quality [1]. As dissolved oxygen levels in water drop below 5.0 mg/l, aquatic life is put under stress; the lower the concentration, the greater the stress. Oxygen levels that remain below 1-2 mg/l for a few hours can result in high mortality rates for fish. Moreover, oxygen affects a vast number of other water indicators, not only biochemical but aesthetic ones like the odour, clarity and taste [2]. Consequently, there is a need to measure this analyte within a single drop of water, upon economical and disposable electrodes.

In view of this requirement, sensors persist to make significant impact in daily life. There has been a strong demand for producing highly sensitive, selective, responsive, and cost effective sensors. As a result, research emphasis is on for developing new sensing materials and technologies. In this context, the use of nanomaterials for the construction of sensing devices constitutes one of the most exciting approaches [3-5]. The extremely promising prospects of these devices accrue from the unique properties of nanomaterials which include extremely high surface to volume ratio, mechanical strength, toughness and electrical or thermal conductivity that allows the achievement of enhanced analytical performance with respect to other materials. With the advent of nanotechnology, research is also on track to create miniaturized sensors. As the world of electronics become smaller, nanoparticles are important components in the chip design. Miniaturized sensors can allow

lower power consumption, reduced weight, low cost and can be used for immediate monitoring in real samples "in the field". With the increased demand for de-centralized sensing traditional techniques utilising highly expensive, immovable analytical equipments such as Gas Chromatograph, Mass Spectrometers are not feasible for sensing outside the realms of standard laboratories [6]. In this context, sensors prepared using screen-printed electrodes (SPEs) using nanostructures offer advantages due to their scales of economy, ease of fabrication, facile modification and disposable nature [7-10].

The anthraquinone and their derivatives have been used as redox active materials for oxygen detection but electrochemistry reported is very poor [11]. The reduction of quinone group causes the formation of semiquinone intermediate which facilitates the oxygen reduction process [12]. Hence, it would be desirable to modify this mediator with nanomaterials which can improve the electrochemistry and performance of the sensor. Gold nanoparticles (GNPs) are designed for use as conductors from printable inks to electronic chips [13]. Nanoscale GNPs are being used to connect resistors, conductors and other elements of an electronic chip. Extending our previous work [11] further for developing a technology we have prepared a material using nanostructured GNPs which was functionalized with anthraquinone-2-COOH/Cysteamine (AQ-Cyst) moiety forming AQ-Cyst moiety functionalized GNPs. Further, these AQ- Cyst moiety functionalized GNPs has been mixed with graphite screen-printable inks to prepare screen-printed bulk modified electrodes which have been applied in the detection of dissolved oxygen.

## 2. Experimental:

### 2.1 Reagents and Materials:

Hydrogen trichloroauratetrihydrate ($HAuCl_4$) were purchased from Aldrich (USA).Anthraquinone-2-carboxylic acid (AQ-COOH), 1-ethyl-3-(3-dimethylaminopropyl) carbodiimide hydrochloride (EDC), N-hydroxysulfosuccinimide (NHS) and cysteamine were purchased from Sigma (USA). All other chemicals employed were of analytical grade. All the solutions were prepared with triple distilled water. All the experiments were performed in 0.1 M phosphate buffer solution (pH 7.1).

### 2.2 Instruments:

The voltammetric measurements were carried out using m-Autolab III (ECO-Chemie, The Netherlands) potentiostat. Cyclic voltammetry studies were performed in electrochemical cell with three electrode system including modified screen-printed electrode as a working electrode, an Ag/AgCl reference electrode and Pt as counter electrode. All electrochemical measurements were carried out in 7 mL phosphate buffer solution, pH 7.1 and deaerated by bubbling pure nitrogen for 15 minutes prior to the experiments. Connectors for the efficient connection of the screen printed electrochemical sensors were purchased from Kanichi Research Services Ltd (UK, http://kanichi-research.com/). TEM measurements of GNPs and AQ functionalized GNPs was performed on a TecnaiG2 (200 kv) instrument. The samples were dispersed in distilled water and deposited onto copper grid for TEM measurements.

### 2.3 Preparation of AQ/ cysteamine moiety functionalized GNPs electrode:

#### 2.3.1. Preparation of GNPs:

In a typical experiment, before preparation of GNPs, apparatus used was pre-cleaned in chromic acid solution. Then aqua regia *(3:1 HCl /$HNO_3$)* was used for cleaning and finally,

all the apparatus was thoroughly rinsed with distilled water. GNPs was prepared by citrate method as reported [14]. 5 mL of 1 mM of hydrogen trichloroaurate trihydrate solution was prepared in a round bottom flask and was vigorously boiled with stirring, fitted with reflux condenser. Then 0.5 mL of sodium citrate (38.8 mM) was added quickly. The solution was refluxed for 15 minutes. The solution was cooled to room temperature and stirred continuously. The prepared GNPs were characterized using Transmission Electron Microscopy (Fig.1A).

**2.3.2 Preparation of AQ-Cyst complex and AQ-Cyst/GNPs :**

AQ-Cyst complex was prepared by carbodiimide coupling reaction process. In this process, 11.6 mg of AQ-COOH was suspended in 700 µL of HEPES [2-{4-(2-hydroxyethyl) piperazin-1-yl}ethanesulfonic acid] buffer solution. To this solution, 44 mg of NHS and 60 mg of EDC were added. The solution was stirred for 45 minutes. 100 µL of cysteamine was added dropwise along with vigorous stirring and the mixture was left at room temperature for 24 hours. Conjugate was washed with water several times, centrifuged and dried in a dessicator. Further, GNPs were added to AQ-Cyst complex for preparation of AQ/ Cyst moiety functionalized GNPs (which will be further referred to as AQ-Cyst/GNPs) and ultrasonication was done for 30 minutes in a bath. The prepared material was washed with triple distilled water, filtered and dried and was further used for TEM analysis.

**2.3.3. Preparation of AQ-Cyst/GNPs bulk modified screen-printed electrodes:**

Screen-printed carbon electrodes were fabricated in-house with appropriate stencil designs using a microDEK1760RS screen-printing machine (DEK, Weymouth, UK). A carbon-graphite ink formulation previously utilised [15] was first screen-printed onto a polyester flexible film (Autostat, 250 mm thickness). This layer was cured in a fan oven at 60

degrees for 30 minutes. Next a silver/silver chloride reference electrode was included by screen printing Ag/AgCl paste (Gwent Electronic Materials Ltd, UK) on to the plastic substrate. Last a dielectric paste ink (Gwent Electronic Materials Ltd, UK) was printed to cover the connections and define the 3 mm diameter graphite working electrode. After curing at 60 degrees for 30 minutes the screen-printed electrode is ready to use. For the preparation of AQ-Cyst/GNPs bulk modified screen-printed electrodes, the prepared AQ-Cyst/GNPs material in the preceding section was further used. The AQ-Cyst/GNPs was incorporated into the screen printed electrodes on the basis of weight % of $M_p$ and $M_I$ where $M_P$ indicate the mass of particulate and $M_I$ indicates the mass of ink formulation used in the printing process respectively [16-17]. Typically, the weight % of $M_p$ and $M_I$ can vary over the range of 0 – 10%. We have used 0.75 % ($M_P/M_I$ = 0.02/2.66 x 100) AQ-Cyst/GNPs for the fabrication of screen printed electrode.

This was then printed on top of the working electrode and cured as described above.

## 3. Results and discussion:

### 3.3.1 Mechanism for formation of AQ-Cyst/GNPs nanohybrid:

To link cysteamine with AQ-COOH, EDC and NHS were used. In this reaction, EDC activates the terminal –COOH groups of AQ-COOH forming a highly reactive O-acyl urea active intermediate. Further, surface of O-acylurea transforms by nucleophilic attack of NHS to form succinimidyl ester with the release of urea as a by-product. A subsequent nucleophilic attack by primary nitrogen of amino compound (cysteamine) to the succinimidyl ester brings about the formation of the amide linkage as indicted in Scheme I. Chemical adsorption of normal thiol derivatives to the particle surface of GNPs occurs via Au-S bonding. The bonding of thiol group to GNPs helps in maintaining the stability of prepared composite after modification without a need for additional additives.

### 3.3.2 Transmission Electron Microscopy:

Transmission electron microscopy image of the prepared GNPs is shown in Fig.1A. Before preparation of composite, average size of spherical GNPs was about 17 nm and after composite preparation, average size changed to 24-25 nm (Fig.1B). This shows the AQ–Cyst complex was deposited on the surface of GNPs by gold-thiol bonding. The results are further supported by the selected area electron diffraction patterns of pure GNPs (Fig. 1C) and AQ-Cyst/GNPs (Fig. 1D) respectively while inset to Fig. 1 C and D, displays the photograph of pure colloidal GNPs and AQ-Cyst functionalized GNPs respectively. The selected area electron diffraction patterns of pure GNPs appear as regular arrays of spot which is proposed to be due to single crystal specimen of GNPs oriented in such a way that several sets of planes are parallel to beam resulting in diffraction pattern consisting of regular arrays of spot [18] suggesting crystalline nature of the GNPs. The selected area electron diffraction patterns of AQ-Cyst/ GNPs, show Scherrer ring patterns associated with the [111], [200], [222] and [311] atomic planes revealing polycrystalline face centered cubic lattice behaviour of AQ-Cyst functionalized GNPs [19,20].

### 3.3.3 Energy Dispersive X-ray:

Fig. 2 shows the energy dispersive X-Ray data for AQ-Cyst/GNPs nanohybrid. EDX analysis was carried out to determine the composition of the prepared material. The results indicate that layer contains mixture of carbon, gold, sulphur and oxygen; least amount being of sulphur and highest amount of carbon. This supports the formation of composite as indicated in Fig. 2 which shows about 91% of C and subsequent percentage of other species.

### 3.3.4 Electrochemical studies:

The electrochemical characterizations of AQ-COOH/GCE and AQ-Cyst/GCE systems were studied in detail and results obtained are shown as Fig. 3A and Fig. 3B respectively. The figure shows positive and negative peaks corresponding to reduction and oxidation reaction attributed to the redox couple $AQ/AQH_2$ (Quinone to hydraquinone) respectively. As indicated in Fig. 3A and 3B, the anodic peak potential $E_a$ and cathodic peak potential $E_p$ of AQ-COOH/GCE system appears to be $E_a$ = -0.246 V and $E_c$ = -0.378 V; while the anodic and cathodic peaks of AQ-Cyst/GCE system was found to be $E_a$ = -0.331 and $E_c$ = -0.519 V at 10 mV/s respectively. The peak separations of AQ-COOH/GCE and AQ-Cyst/GCE was found to be 132 and 188 mV at 10 mV/s scan rate showing that the process is quasireversible at slower scan rate. Formal potential calculated from the midpoint of cathodic and anodic peaks is found to be -0.312 V and -0.425 V. The inset to Fig. 3A and 3B shows the peak current vs. scan rate plot where the peak current $i_p$ for oxidation and reduction was found to be linear with the scan rates showing surface-controlled electrochemical reaction at both the electrodes. On attaching the GNPs to AQ-Cyst complex, the peak separation decreases to 113 V at 10 mV/s which clearly shows better electrochemistry and facile electron transfer for the AQ-Cyst/GNPs/CS/GCE system. Further it can be observed on comparing the data's of AQ-COOH system to AQ-Cyst system and AQ-Cyst/GNPs system; there is a maximum increase in peak current and decrease in peak separation for AQ-Cyst/GNPs clearly indicating that the GNPs plays a very important role in the electron transfer process. The increase in electron density after addition of GNPs might be due to increase in surface area and decreased leaching of mediator compared to AQ-COOH and AQ-Cyst systems.

Fig. 4A and 4B, indicates that the oxidation and reduction potentials follow a linear relation with logarithm of scan rates for AQ-COOH and AQ-Cyst systems similar to the Laviron's theory which can be represented as indicated in equations (i),(ii) and (iii):

$$E_{pa} = E^o + X \ln [(1 - \alpha) F\nu/RTk_s] \qquad \text{(i)}$$

$E_{pc} = E^o + Y \ln [(\alpha) F\nu/RTk_s]$ (ii)

$\ln k_s = \alpha \ln(1- \alpha) + (1 - \alpha)\ln \alpha - \ln (RT/nF\nu) - \alpha (1- \alpha) nF\Delta Ep/RT$ (iii)

Where α, $k_s$ and ν are the electron transfer coefficients, apparent charge transfer rate constant and potential sweep rates, respectively. The slope of the anodic peak potential ($E_{pa}$) and cathodic peak potential ($E_{pc}$) vs log scan rates are found as X = RT/ (1 - α)nF and Y = RT/ αnF, respectively. Table 1 compares the kinetic parameters for different electrodes. The electron transfer coefficient (*α*) and charge transfer rate constants, $K_s(S^{-1})$ were found to be 0.61 and 1.4 respectively for AQ-Cys/GCE; and 0.73 and 0.70 respectively for AQ-COOH/GCE systems.

In a similar way, the electron transfer coefficient (α) and charge transfer rate constants, $K_s$ ($S^{-1}$) were found to be 0.56 and 4.8 respectively for AQ-Cys/GNPs/GCE [21] and 0.48 and 5.23 respectively for AQ-cyst/GNPs/SPE. The value for electron transfer rate constant for AQ-Cyst/GNPs/SPE is higher than the apparent heterogeneous electron transfer rate constant of various systems AQ-COOH/GCE, AQ-Cyst/GCE and AQ-Cyst/GNPs/GCE, showing that the electron transfer at AQ-Cyst/GNPs/SPE is more facile, indicating suitability of prepared material for electrochemical applicability for constructing SPEs.

Fig.5 A shows the cyclic voltammogram of AQ-Cyst/GNPs/GCE and Fig.5B shows the cyclic voltammogram of AQ-Cyst/GNPs/SPE at scan rate of 10 mV/s. The anodic and cathodic peaks were found to be at potentials 0.714 V (vs. Ag/AgCl) and 0.115 V (vs. Ag/AgCl) for AQ-cyst/GNPs/SPE. On comparing the two electrodes it could be clearly inferred that on incorporating the AQ-Cyst/GNPs nanomaterial on SPEs, the voltammetric peaks noted in the cyclic voltammogram shift significantly towards more positive potential which eliminates the possibility of interference from other analytes which are readily reduced at more negative potentials.

**3.3.5. Electrochemical reduction of dissolved oxygen on AQ-Cyst/GNPs/SPE:**

The typical oxygen reduction reaction (ORR) involve two electron transfer to produce hydrogen peroxide while the four electron transfer result in the formation of water and involve $O_2/O_2^-$ reaction at equilibrium followed by disproportionation of the superoxide anion or to a slow chemical step following the first electron transfer where reaction step two is rate determining step at carbon surface [22]. Supplementary material indicates the oxygen reduction on bare glassy carbon electrode occurs at very high over potential i.e. near -0.8 V [21]. However, the pretreatment of GCE causes the oxygenated group formation on carbon surface which facilitate the electron transfer and decrease the overpotential of ORR to some extent. In this context, the quinone based compounds possessing π-electrons and reducible p-quinone system which can involve in electron transfer reaction and decrease the overpotential required for activation, are quite useful to act as redox mediator. The probable mechanism of electron transfer pathway in oxygen reduction reaction is shown below [12, 21, 22, 24, 25]. The mechanism depicts electrochemically generated radical anion/semiquinone species (eq. (iv), where Q means a quinone species attached/adsorbed to a carbon electrode surface) reacts with molecular oxygen, forming an intermediate superoxo species ($O_2^{\bullet -}$, eq. (v)). Reaction (v) is rate determining and in this reaction model, the overall rate is determined by the surface concentration of Q•− [22, 23]. Reactions (vi) and (vii) are considered to be fast and lead to the formation of peroxide although the preferred route to peroxide is most likely the further reaction of the $O_2$•− intermediate [26].

Step (I): Formation of quinone radical anion

$$Q + e^- \rightarrow Q^{\bullet -} \qquad \text{(iv)}$$

Step (II): Formation of superoxide ion (Rate determining step)

$$Q^{\bullet -} + O_2 \xrightarrow{K_c} O_2^{\bullet -} + Q \qquad \text{(v)}$$

Step (III): Disproportionation reaction

$2O_2^{\bullet-} + H_2O \rightarrow O_2 + HO_2^- + OH^-$ (vi)

Or

Step (IV): Reduction of $O_2$ at the electrode

$O_2^{\bullet-} + H_2O + e^- \rightarrow HO_2^- + OH^-$ (vii)

where Q denotes surface quinone species.

Fig. 6 indicates the response of AQ-Cyst/GNPs/SPEs on addition of increasing concentrations of oxygen which was passed through solution of 0.1 M phosphate buffer solution, pH 7.1 after purging with nitrogen. Fig. 7 shows the calibration plot for AQ-Cyst/GNPs/SPEs. The electroanalytical determination of dissolved oxygen is found to be possible over the concentration range of 0.2 mg/L to 6.1 mg/L with a detection limit of 0.131 mg/L (based on 3-sigma). After 6.1 mg/L the current moves towards saturation point. To the best of our knowledge no report is available for detection of oxygen to such low levels using screen-printed design indicating the suitability of the prepared material for determination of dissolved oxygen (Table 2).

### 3.3.6 Performance of sensor

The stability of the electrode was studied electrochemically by using cyclic voltammetry. To study the stability of AQ-Cyst/GNPs/SPEs, 25 repeated cycles were scanned but no appreciable change was observed in the cyclic voltammogram of the modified electrode which justifies the stability of present AQ-Cyst/GNPs modified screen-printed electrode. When 25 continuous cycled scans were carried out at 20 mV/s scan rate a 5% decrease of the initial response at 0.4 mg/L of oxygen was observed. The RSD of 2.5% was observed for three successive measurements of one AQ-Cyst/GNPs modified electrode at 0.4 mg/L oxygen indicating good reproducibility of the proposed dissolved oxygen sensor. The long term stability of the proposed sensor was also studied. The lifetime of the SPEs (when

not in use) was determined to be greater than 4 months when the electrode was kept in an oxygen free environment. The screen-printed electrodes were also used for the analysis of real water samples (pond water and tap water).The results obtained were in good agreement with results obtained using Winkler's method which confirms the suitability of the prepared electrode (Table 3). The effort is on for further technology development. A patent has been applied for the prepared material [37].

## 4. Conclusions:

We have demonstrated the successful electrochemical detection of dissolved oxygen utilising a AQ-Cyst/GNPs modified screen-printed bulk modified electrode. The sensor which allows for excellent reproducibility for the sensing of the analyte coupled with its ease of fabrication, mass production and importantly, low cost provides a real possibility for the development of a 'real-world' electrochemical sensing device for the monitoring of dissolved oxygen at very low levels.

**Acknowledgement:**

The present work has been performed by funds sanctioned UGC-UKIERI Thematic Partnerships. The authors are grateful for this financial support. The author is also highly grateful to Prof. O.N. Srivastava and Mr. Dinesh, Department of Physics, BHU, Varanasi for providing TEM facility.

**References:**


1. M.K. Stenstorm, *Water Research*, 1980, **14,** 643–649.

2. P. R. Kannel, S. Lee, Y. S. Lee, S. R. Kanel, S.P. Khan, *Envirn. Monit. Assess*., 2007, **132** 93-110.

3. A. Miguel, C. Duarte, L.M.L. Marzan, *J. Mater. Chem.*, 2006, **16**, 22–25.

4. D. Eder, *Chem. Rev.*,2010, **110,** 1348–1385.

5. Q. Li, Y. Li, X. Zhang, B.S. Kumar, C. Annanavar, Y. Zhao, M. Andrea, D.L. Zheng, S.K. Doom, Q. Jia, D.E. Peterson, P.N. Arendt, Y. Zhu, *Adv. Mater.*, 2007, **19,**3358–3363.

6. K. Z. Brainina, *Anal. Chem.*, 2001, **56**, 303-312.

7. J. P. Hart,S. A. Wring, *Trends Anal. Chem.*, 1997, **16**, 89-103.

8. J. P. Hart,S. A. Wring, *Electroanalysis*, 1994, **6** 617-624.

9. M. A. Sirvent, A. Merkoci S. Alegret, *Sens. Actuat. B*, 2000, **69,** 153-163.

10. A. Morrin, A. J. Killard, M. R. Smyth, *Anal. Lett.*, 2003, **36**,2021 - 2039.

11. I. Tiwari, M. Singh, M. Gupta, S.K. Aggarwal, *Mat. Res. Bull.*, 2012, **47,** 1697–1703.

12. G. Jurmann, D. J. Schiffrin, K. Tammeveski, *Electrochim. Acta.,* 2007, **53**, 390–399.

13. D. Huang, F. Liao, S. Molesa, D. Redinger, V. Subramanian, *J. Electrochem. Soc.*, 2003, **150**, G 412-417.

14. I. Tiwari, M. Gupta, Mat. Res. Bull., 2014, **49**, 94-101.

15 R. O. Kadara, N. Jenkinson, B. Li, K. H. Church, C. E. Banks, *Electrochem. Commun.*, 2008, **10**, 1517- 1519.

16. R. O. Kadara, N. Jenkinson, C. E. Banks, *Electroanalysis*, 2009, **21**, 2410-2414,

17. M. Khairy, R. O. Kadara, D. K. Kampouris, C. E. Banks, *Electroanalysis*, 2009, **21,** 1455 – 1459.

18. Peter J. Goodhew, John Humphreys, Richard Beanland, Electron Microscopy and Analysis, Third Edition, CRC Press, Pages 254, 2000.

19. Absar Ahmad, Satyajyoti Senapati, M. Islam Khan, Rajiv Kumar and Murali Sastry, *Langmuir* 2003, *19,* 3550-3553

20. Sujoy K. Das,a Calum Dickinson,b Fathima Lafir,b Dermot F. Broughamc and Enrico Marsili, *Green Chem.*, 2012, 14, 1322-1334.

21. I. Tiwari, M. Gupta, R. Prakash, C. E. Banks, *Anal. Meth.*, 2014, **6**, 8793-8801.,

22. K. Tammeveski, K.S. Kontturi, R.J. Nichols, R.J. Potter, D.J. Schiffrin, *J. Electroanal. Chem.*, 2001, **515**, 101–112.

23 M.S. Hossain, D. Tryk, E. Yeager, *Electrochim. Acta* 34 (1989) 1733.

24. C.E. Banks, G.G. Wildgoose, C.G.R. Heald, R.G. Compton, *J. Iranian Chem. Soc.,* 2005, **2**, 60-64.

25. Marko Kullaperea, Jaanika-Maria Seinberga, Uno Mäeorga, Gilberto Maiab, David J. Schiffrin c, Kaido Tammeveskia, *Electrochim. Acta* 54 (2009) 1961–1969.

26. J.R.T.J. Wass, E. Ahlberg, I. Panas, D.J. Schiffrin, *Phys. Chem. Chem. Phys.* 8 (2006) 4189.

27. R. S. Tieman, W. R. Heineman, *Anal. Lett.* 1992, **25,** 807-819.

28. L. Shitanda, S. Mori, M. Itagaki., *Anal Sci.*, 2011, **27**, 1049-52.

29. R. J. Zheng, Y. M. Fang, S. F. Qin, J. S. A. H. Wu, J. J. Sun, *Sens. Actuat. B: Chemical*, 2011, **157**, 488–493.

30. J. M. Zen, Y. S. Song, H. H. Chung, C. T. Hsu, A. S. Kumar, *Anal. Chem.*, 2002, **74,** 6126-3.

31. Y. Z. Lam, J. K. Atkinson, *Med. Biol. Eng. Comp.*, 2003, **41**, 456-463.

32. J. Lee, M. Krishnan, A. Damien, S. D. Debbie http://doi.org/10.1016/j.electacta.2012.09.104

33. Y. Xiong, J. Xu, J.W. Wang, Y.F. Guan, *Anal. Bioanal. Chem.* 394 (2009) 919–F923.

34. Y. Xiong, J. Xu, D.Q. Zhu, C.F. Duan, Y.F. Guan, *J. Sol Gel Sci. Technol.* 53 (2010) 441–447.

35. F.S. Damos, R.C.S. Luz, A.A. Tanaka, L.T. Kuboto, *Anal. Chim. Acta* 664 (2010) 144–150

36. J.C.R. Duarte, C.S. Luz, F.S. Damos, A.A. Tanaka, L.T. Kubota, *Anal. Chim. Acta* 612(2008) 29–31.

37. I. Tiwari, M. Gupta, R. Prakash, Patent No. 3150/DEL/2013 dated 23.10.2013

Table 1: Kinetic parameters for the fabricated electrodes:

| Sl No. | Electrodes | Electron transfer coefficient (α) | Charge transfer rate constants, $K_s$ ($S^{-1}$) | Surface coverage area (mol $cm^{-2}$) |
|---|---|---|---|---|
| 1. | AQ-Cys/GNPs/GCE | 0.56 | 4.7 | $12 \times 10^{-9}$ |
| 2. | AQ-Cys | 0.61 | 1.4 | $2.9 \times 10^{-10}$ |
| 3. | AQ-2-COOH | 0.73 | 0.70 | $4.1 \times 10^{-10}$ |
| 4. | AQ-Cys/GNPs/SPE | 0.48 | 5.2 | - |

Table 2: Comparison of linear range and detection limit of some modified electrode and AQ-Cyst/GNPs nanohybrid modified screen printed electrode for the dissolved oxygen sensor

| Serial no. | Type of sensor construction | Technique | sensitivity | Linear range (mg $L^{-1}$) | Detection limits (mg $L^{-1}$) | References |
|---|---|---|---|---|---|---|
| 1. | Pt/SPEs | Amperometry | - | 0-100% | - | [27] |
| 2. | Cerium oxide/silver Catalyst/PDMS/SPE | - | -158 µA mM | - | 8.4 µM | [28] |
| 3. | CdS-SPCEs | ECL | - | 1.7–33 | 0.02 | [29] |
| 4. | Cu-SPEs | - | 23.51µA $cm^{-1}$ | 1-8 | - | [30] |
| 5. | Clark cell Implemented SPEs | CV | 0.02 µAmmHg$^{-1}$ | - | - | [31] |
| 6. | RTIL-SPEs | CV | - | 10–100% | | [32] |
| 7. | Hybrid fluorinated Xerogels /$[Ru(bpy)_3]^{3+}$ | optical | - | 0.0–40.0 | 0.05 | [33] |
| 8. | Ru(II)/fluorinated xerogel | optical | - | 0.0–40.0 | 0.04 | [34] |
| 9. | βCDSH/FeTMPyP /βCDSHAuNP | | 5.5 | 0.2–6.5 | 0.02 | [35] |
| 10. | FeTsPc/FeT4MPyP-modified electrode | RDE and CV | 4.12 | 0.2–6.4 | 0.06 | [36] |
| 11. | AQ-Cyst/GNPs/CS /SPEs | CV | - | 0.2-6.1 | 0.131 | Present work |

Table 3: Determination of dissolved oxygen in water samples by the AQ-Cyst/GNPs nanocomposite modified SPE electrode and Winkler's method

| Sample Name | AQ-Cyst/GNPs/SPE nanocomposite modified SPE (ppm) | Winkler's method (ppm) |
|---|---|---|
| Pond water | 4.4(±0. 50)(n=3) | 4.6 (±0.50)(n=3) |
| Tap water | 4.1(±0.60)(n=3) | 4.5(±0.60)(n=3) |

**Figure captions:**

Fig. 1: Transmission electron microscopy image of (A) prepared GNPs; (B) AQ-Cyst/GNPs nanohybrid; (C) diffraction pattern of GNPs; Inset: Photograph of prepared GNPs (D) diffraction pattern of AQ-Cyst/GNPs nanohybrid; Inset: Photograph of AQ-Cyst functionalized GNPs

Fig. 2: Energy Dispersive X-ray data of AQ-Cyst/GNPs nanohybrid.

Fig.3: Cyclic voltammograms of (A) AQ-COOH/GCE and (B) AQ-Cyst/GCE in 0.1M nitrogen saturated phosphate buffer (pH 6.5) ; Insets: Peak current ($i_p$ ) vs. Scan rates (ν) plot.

Fig. 4: Laviron's plot of (A) AQ-COOH/GCE (B) AQ-Cyst/GCE in 0.1 M PBS (pH 6.5)

Fig. 5A Cyclic voltammogram of (a) Bare GCE (b) AQ-Cyst/GNPs/GCE in 0.1M nitrogen saturated phosphate buffer (pH 6.5).

Fig. 5B: Cyclic voltammogram of AQ-Cyst/GNPs/SPE in 0.1 M nitrogen saturated phosphate buffer (pH 7.1).

Fig. 6: Cyclic voltammetric response of 2.58 mg/L and 4.20 mg/L of oxygen at bare GCE (green and blue line) and at AQ-Cyst/GNPs/SPEs (black and red line) respectively in 0.1 M phosphate buffer (pH 7.1) after purging with nitrogen.

Fig. 7: Calibration plot for AQ-Cyst/GNPs/SPEs.

Scheme I: Mechanism for formation of AQ-Cyst complex.

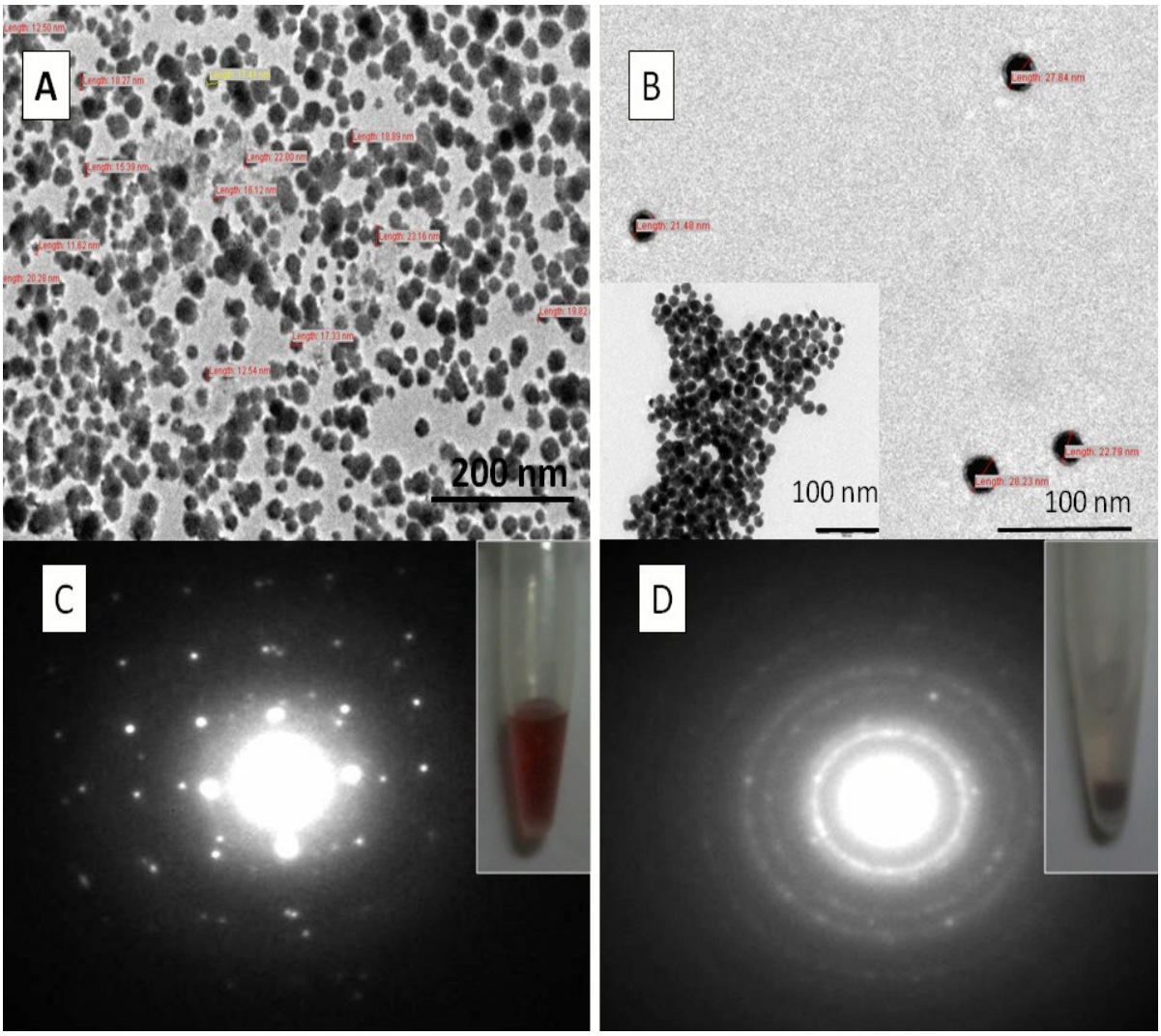


**Fig. 1:** Transmission electron microscopy image of (A) prepared GNPs; (B) AQ-Cyst/GNPs nanohybrid; (C) Selected area diffraction pattern of GNPs; Inset: Photograph of prepared GNPs (D) selected area diffraction pattern of AQ-Cyst/GNPs nanohybrid; Inset:Photograph of AQ-Cyst functionalized GNPs

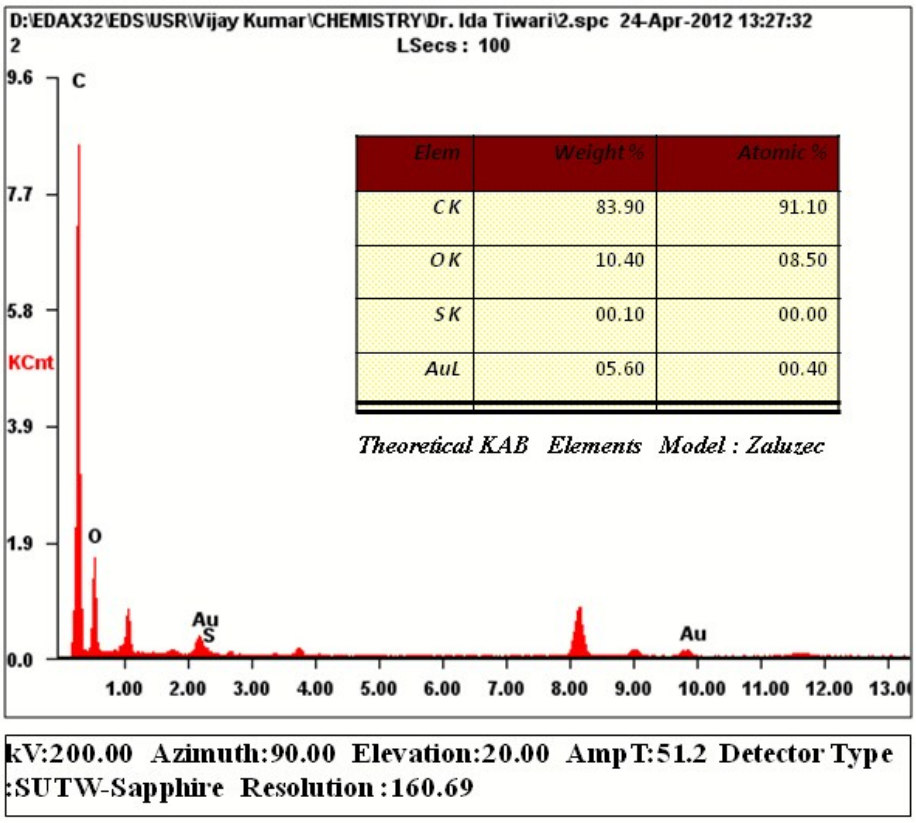


**Fig. 2:** Energy Dispersive X-ray data of AQ-Cyst/GNPs nanohybrid .

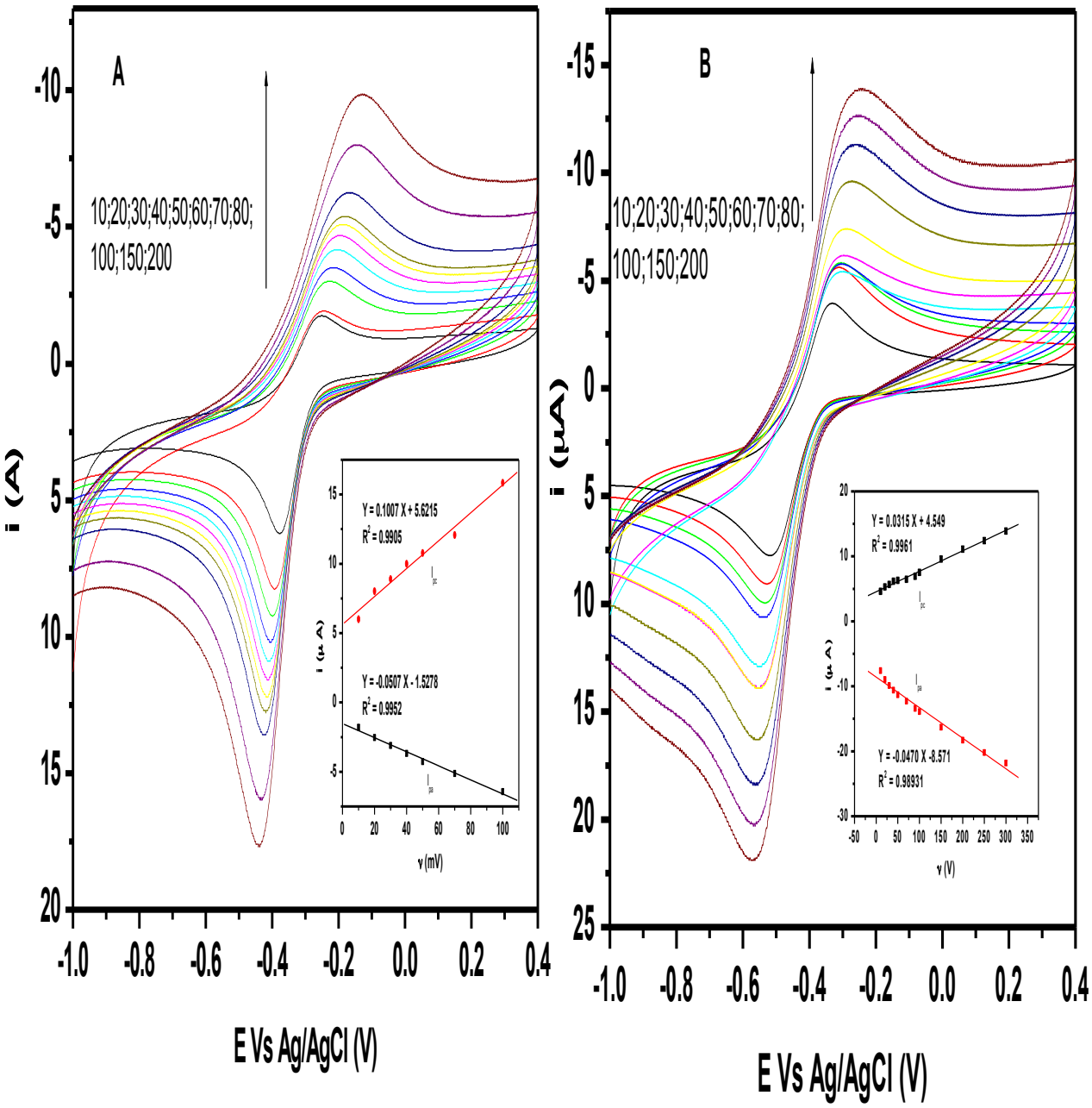


**Fig.3**: Cyclic voltammograms of (A) AQ-COOH/GCE and (B) AQ-Cyst/GCE in 0.1M nitrogen saturated phosphate buffer (pH 6.5) ; Insets: Peak current ($i_p$ ) vs. Scan rates (ν) plot

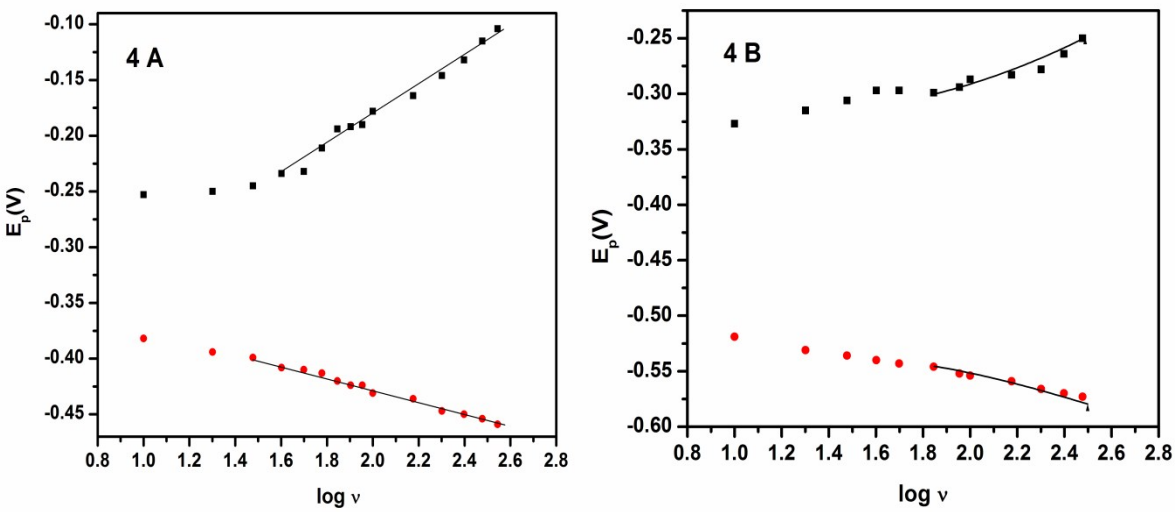


Fig. 4: Laviron's plot of (A) AQ-COOH/GCE (B) AQ-Cyst/GCE in 0.1 M PBS (pH 6.5)

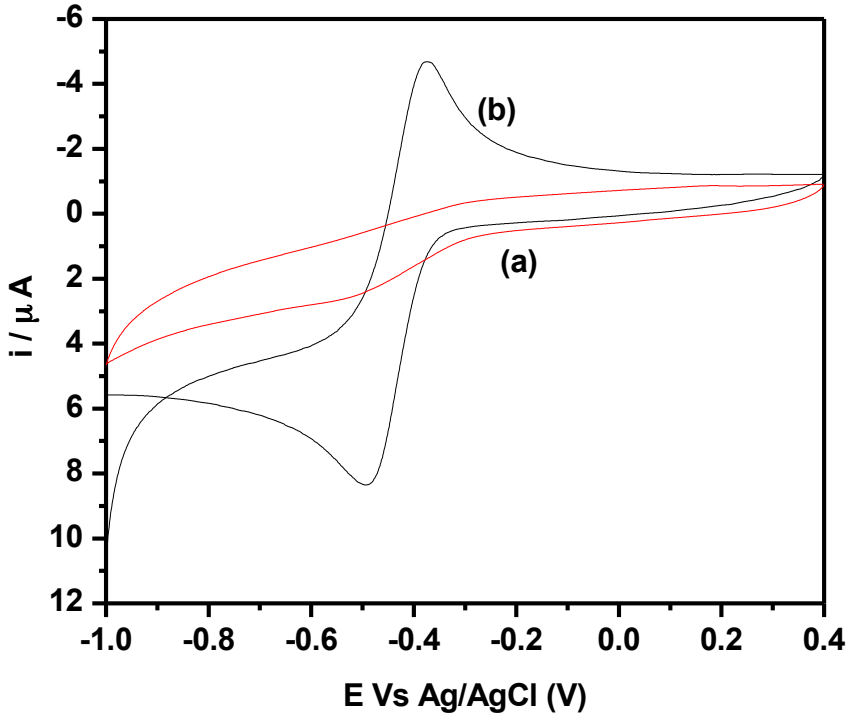


Fig. 5A Cyclic voltammogram of (a) Bare GCE (b) AQ-Cyst/GNPs/GCE in 0.1M $N_2$ saturated phosphate buffer (pH 6.5).

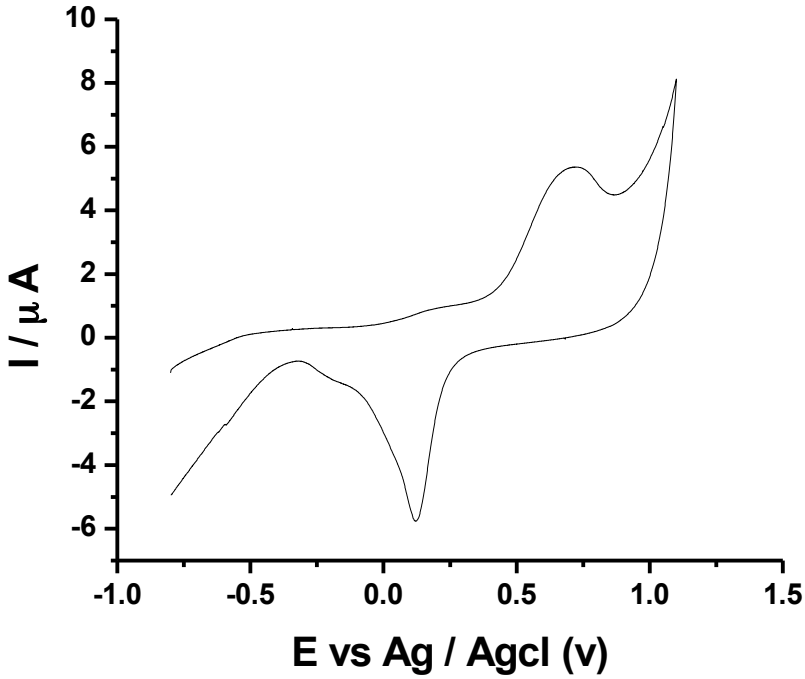


**Fig. 5B:** Cyclic voltammogram of AQ-Cyst/GNPs/SPEs in 0.1 M $N_2$ saturated phosphate buffer (pH 7.1) at 10 mV/s.

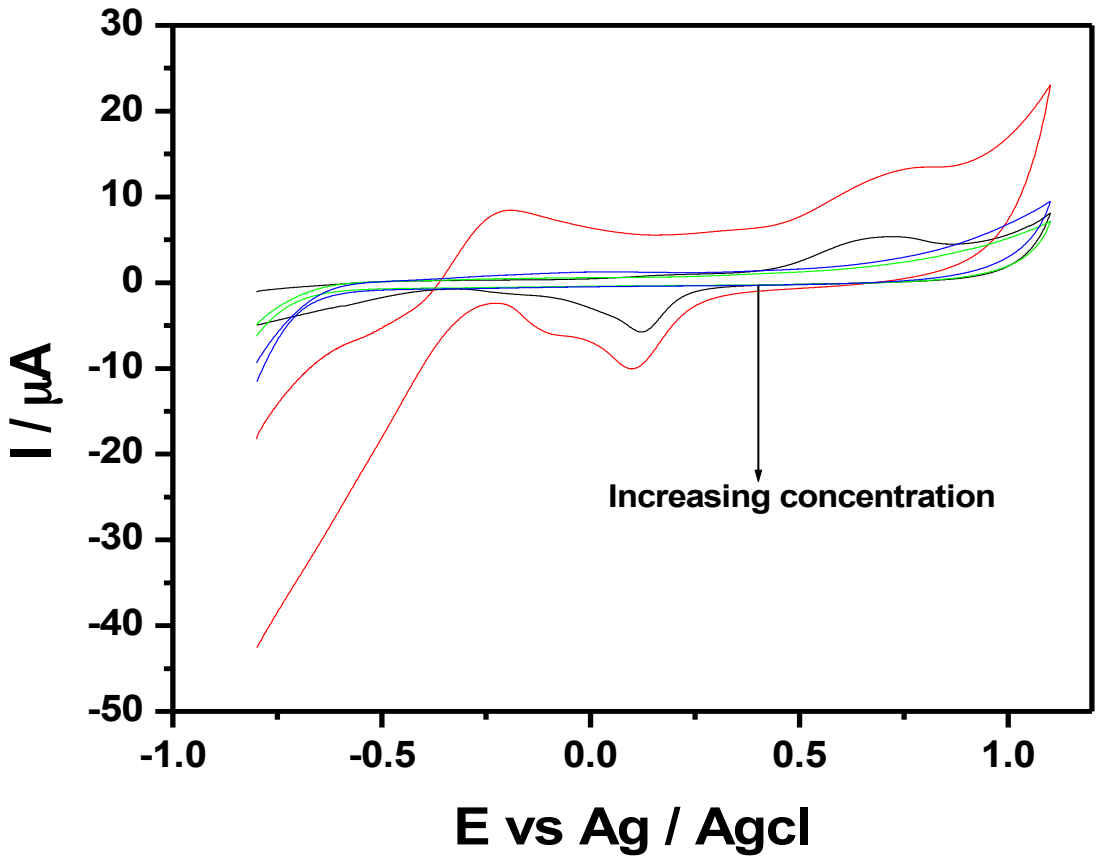


**Fig. 6:**Cyclic voltammetric response of 2.58 mg/L and 4.20 mg/L of oxygen at bare GCE (green and blue line) and at AQ-Cyst/GNPs/SPEs (black and red line) respectively in 0.1 M phosphate buffer (pH 7.1) after purging with nitrogen.

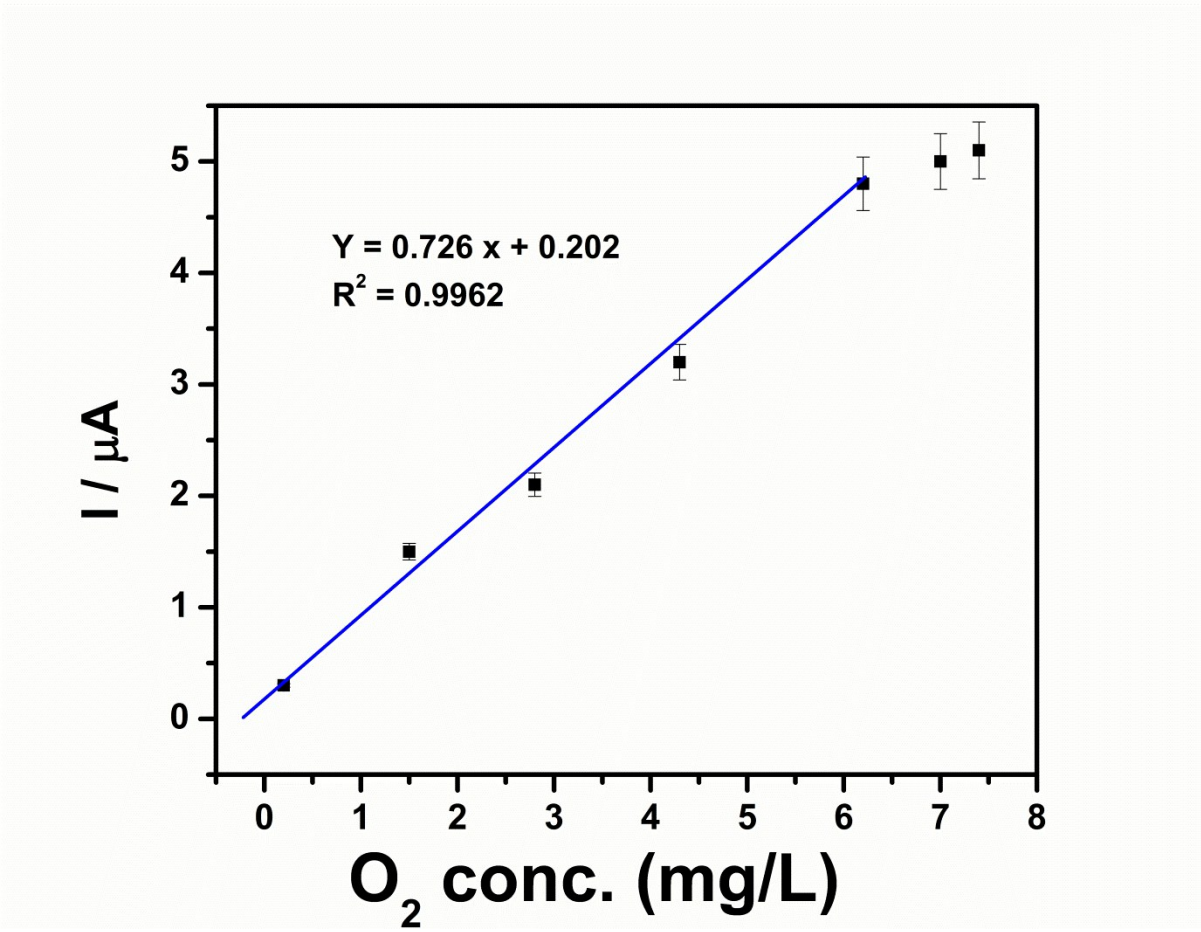


**Fig. 7:** Calibration plot for AQ-Cyst/GNPs/SPEs (i vs $[O_2]$)

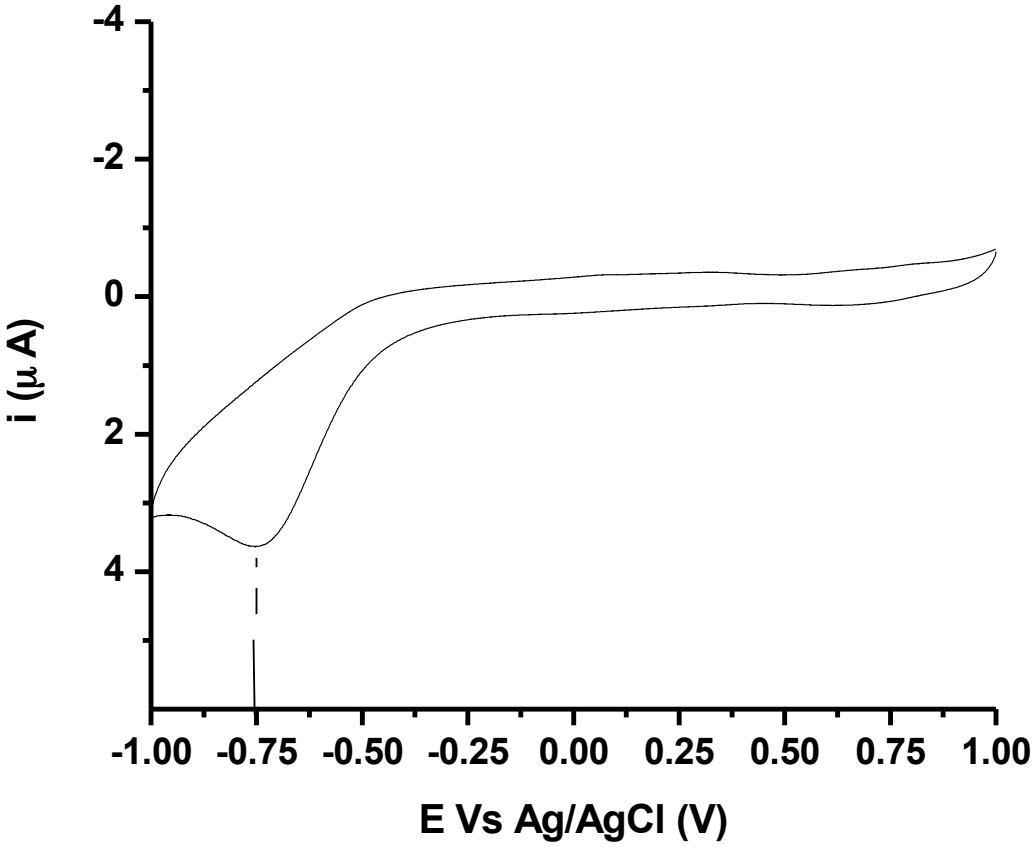


Supplementary material: CV responce of 0.4 mg/L $O_2$ at bare GCE.

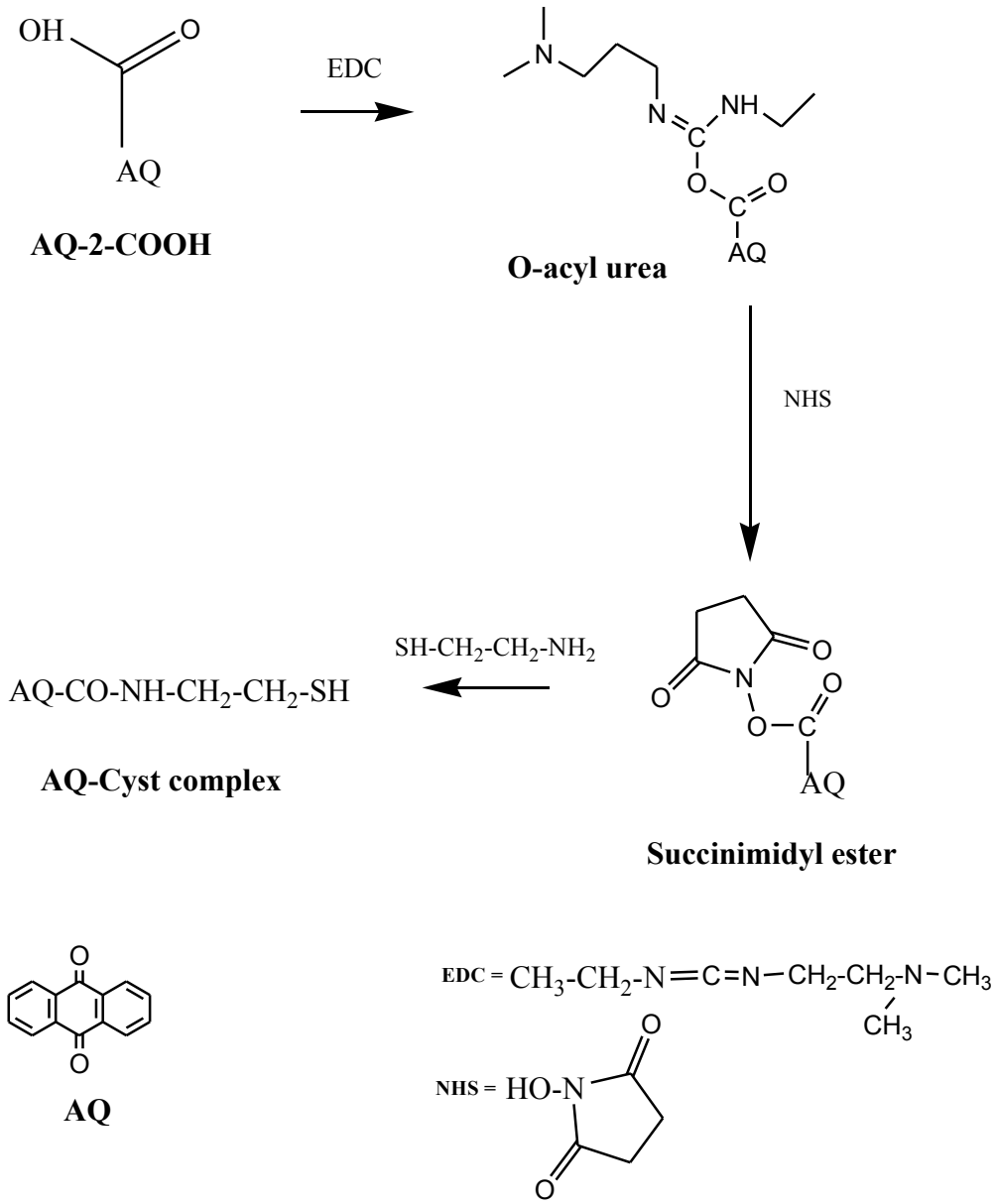


**Scheme I:** Mechanism for formation of AQ-Cyst complex